Selective Anion-Induced Crystal Switching and Binding in Surface Monolayers Modulated by Electric Fields from Scanning Probes

Brandon E. Hirsch, Kevin P. McDonald, Bo Qiao, Amar H. Flood,* and Steven L. Tait*

Department of Chemistry, Indiana University, 800 E. Kirkwood Avenue, Bloomington, Indiana 47405, United States

ABSTRACT Anion-selective (Br^- and I^-) and voltage-driven crystal switching between two differently packed phases ($\alpha \leftrightarrows \beta$) was observed in 2D crystalline monolayers of aryl-triazole receptors ordered at solution–graphite interfaces. Addition of Br^- and I^- was found to stimulate the $\alpha \rightarrow \beta$ phase transformation and to produce ion binding to the β phase assembly, while Cl^- and BF_4^- addition retained the α phase. Unlike all other surface assemblies of either charged molecules or ion-templated 2D crystallization of metal-ligand or receptor-based adsorbates, the polarity of the electric field between the localized scanning tip and the graphite substrate was found to correlate with phase switching: $\beta \rightarrow \alpha$ is driven at -1.5 V, while $\alpha \rightarrow \beta$ occurs at $+1.1$ V. Ion-pairing between the countercations and the guest anions was also observed. These observations are supported by control studies including variation of anion species, relative anion concentration, surface temperature, tip voltage, and scanning time.

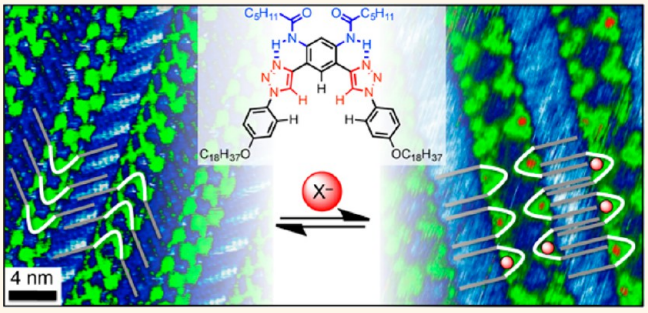

KEYWORDS: anion recognition · scanning tunneling microscopy · self-assembly · supramolecular chemistry · switching

Interest in switchable and self-assembled materials[1] motivates studies of how condensed phases can be programmed to change their structure and function by responding controllably to external stimuli. Two-dimensional (2D) crystalline monolayers that form through noncovalent interactions of molecular building blocks at the interface[2] between electrodes and solutions are ideal for the study of responsive systems.[3] Dynamic equilibria, particularly between solvated and adsorbed states of the molecules, can enable such systems to reorder upon external stimulation when the lattice energy landscape of the packing structure shifts upon introduction of the stimulus. These changes can be observed with submolecular resolution real-space imaging using scanning tunneling microscopy (STM), typically in nonaqueous solutions where the organic adsorbates have optimal solubility. Therein, guest-,[4,5] cation-,[6−11] heat-,[12] shear-,[13] and light-triggered[14,15] transformations between 2D crystalline monolayers have been demonstrated. Despite these recent studies, there remain many unexplored facets of the functionality, dynamics, and response of 2D crystals that incorporate charged components.

The behavior of negatively charged anions at such liquid–solid interfaces is underinvestigated considering that they are present in equal numbers as cations and that they have important impacts in chemistry[16] and biology.[17] For example, chloride salts in crude oil need to be better managed and removed during desalting to reduce the corrosion and catalyst poisoning they can cause during refining.[18] Despite these important needs, elementary studies investigating how anions bind to 2D monolayers of molecular receptors are still in their infancy. In the first example[19] we know of, addition of anions to a crystalline monolayer led to almost complete loss of order. In a second,[20] we observed anion-templated dimer formation with retention of the ordered packing. Neither study provided conclusive evidence of anion binding. Anion-induced crystal switching between ordered phases

* Address correspondence to aflood@indiana.edu, tait@indiana.edu.

Received for review August 20, 2014 and accepted September 25, 2014.

Published online September 25, 2014
10.1021/nn504685t

and visualization of the anion when it is bound to the cavities of surface-adsorbed receptors have not previously been achieved.

Compared with cations (*e.g.*, alkali and transition metals), anions[16] (*e.g.*, halides, BF_4^-, NO_3^-, and PF_6^-) generally are significantly larger in size, have stronger solvation shells, and lack d-orbital participation in bonding, factors that are known[16] to contribute to their weaker binding energies. These aspects must be overcome in order to examine anions at liquid–solid interfaces. For these same reasons, it was monatomic cations that were first utilized to trigger phase transformations[6–11] between 2D crystalline monolayers. Yet it is interesting that, despite this precedence, these cations were never seen clearly by STM imaging in nonaqueous solutions, thus motivating the question of whether they bind to the surface-adsorbed receptors or not. Furthermore, when considering ion binding at interfaces, counterions[7,8] must always be present for charge balance. Only once have counterions been seen; in that case iodide (I^-) appeared[21] during STM imaging of a random 2D cocrystalline array of cationic (pyridinium-based) and neutral adsorbates. It is also surprising that among these cation-binding studies none have been investigated using the traditional approach[22] of titrating the ions into solution but instead have relied upon the addition of a single equivalent of ion. Thus, there is no information available on how the ion-binding properties are changed when the receptors are ordered into either interfacial monolayers or a rigid crystal lattice.

Finally, even though there are many examples[6–11] where STM imaging has been used to study either cation-induced assemblies or the assemblies formed from cationic molecules, none of the ions have been reported to respond to the scanning probe's electric field (*E*-field). This situation could arise from the fact that monatomic cations have never been seen, as noted above. Thus, scanning probe imaging has not previously provided information on the binding and debinding of ions in surface assemblies. Alternatively, it might be easier to observe the after-effect of cation debinding from the surface, such as reversion back to the ion-free assembly following after scanning with the *E*-field. Yet we note that it is only once, and with the use of chemical[11] rather than *E*-field stimulation, that switching between the ion-stabilized and ion-free assembly has been produced. Indeed, ionic bonding in 2D crystals at surfaces by monatomic cations can produce structures with high thermal stability.[23,24] More labile ions may be required to enable responsive behaviors. For this reason, anions might offer the needed dynamic ion debinding on account of their intrinsically weaker binding to receptors.

The principal conditions under which *E*-field-triggered changes[25–35] to the phase behavior have been readily observed are with physisorbed monolayers on gold electrodes that are interfaced with aqueous solutions and when using electrochemical STM. Therein, the charge present at the surface is controlled using the voltage that is applied across the *entire* surface. Voltage-driven changes using only the *localized* and *scanning* STM probe are rare[36–38] despite the number of cationic assemblies.[6–11,38–43] In nonaqueous solutions corresponding to the conditions studies herein, the STM tip polarity has been observed twice to drive switching. First, the orientational alignment[37] of a dipolar, zwitterionic triple-decker compound has been flipped between ordered and disordered phases as programmed using *E*-field polarity. Second, transitions of a cationic polyaromatic compound[36] on highly oriented pyrolytic graphite (HOPG) took place using voltage pulses but could not be programmed because the transformations were independent of polarity.

For all these reasons, we were surprised to discover the first anion-driven crystal switch between two ordered phases, α and β (Figure 1), and to discover that this order–order transition can be stimulated

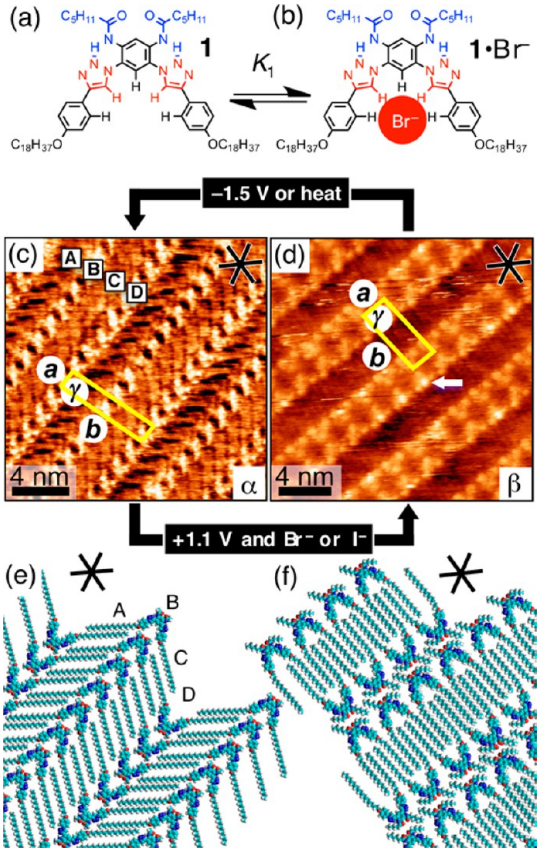

Figure 1. (a) Structure of receptor 1 and (b) formation of the 1·Br⁻ complex. (c) STM image of a 2D crystalline monolayer of 1, α phase, at the octanoic acid–graphite interface ([1] = 1.2 × 10^{-4} M; unit cell: *a* = 1.36 ± 0.08 nm, *b* = 6.49 ± 0.13 nm, γ = 89 ± 2°). (d) STM image of the β phase observed after deposition of an equimolar solution of 1 and TBA·Br ([1] = [Br^-] = 1.2 × 10^{-4} M, unit cell: *a* = 2.00 ± 0.11 nm, *b* = 5.10 ± 0.18 nm, γ = 92 ± 3°). (e) Packing models of the α and (f) β phase structures. (STM: I_T = 10 pA, V_{sub} = (c) −0.7 V and (d) −0.4 V.)

reversibly and locally by the scanning tip (Figure 1d and e). The $\alpha \rightarrow \beta$ switch is selective and could only be produced upon titration of specific anions into solutions of aryl-triazole-based receptors that are organized on the surface of HOPG. We also report the first visualization of a bound anion (Br^-) and a bound ion pair (I^- with tetrabutylammonium, TBA^+). We found that the anion's occupancy and the crystal morphology responded in a reproducible manner to the polarity (+/−) and magnitude of the *E*-field (*e.g.*, −0.7 *versus* −1.5 V) as well as the duration of exposure to the scanning tip (0−2 h). We compare the anion-binding behavior of the receptor in solution to the surface studies in order to provide insight into the factors affecting the selective anion-induced crystal switching of the surface monolayer without an anion-stimulated conformational change of the receptor core.

RESULTS AND DISCUSSION

Herein, we employ anion-binding adsorbates constituted by receptors bearing triazoles[44−47] (red, Figure 1a) for anion complexation and two C_{18} chains at their tails to facilitate formation of monolayers on HOPG. Amides (blue, Figure 1a) at the receptors' head rigidify[45] the crescent-shape structure, allowing them to retain this shape through anion binding and debinding events: In spite of the strong intramolecular clash of the two aligned 5-debye dipoles localized on the triazoles in this conformation (which helps create the strong anion affinity in the receptor cavity[45]), the *syn* arrangement of the receptor core is preferred. This conformational predisposition has been verified by geometry optimization using density functional theory at the B3LYP/6-31G* level of theory (Figures S1−S3) and by solution phase characterization using ^{1}H NMR-based nuclear Overhauser effect spectroscopy. This conformational simplicity is an important structural element in this study that allowed us to focus solely on the impacts of anion binding and STM bias manipulation on the supramolecular assembly.

Anion Binding Drives Changes to the Packing: $\alpha \rightarrow \beta$. Receptor **1** was found to form an ordered α phase constituted by lamella arranged in *anti*-parallel rows at the octanoic acid−HOPG interface. High-resolution STM images (Figure 1c) show rows (B and D) of bright aryl-triazole cores aligned head-to-tail and spaced apart by darker rows (A and C) of alkyl chains interdigitated with the neighboring *anti*-parallel rows. A corresponding 2D crystal structure has been proposed (Figures 1e and S4). The orientation of the crystal structure with respect to the underlying graphite lattice can be determined precisely by changing the imaging bias to −0.002 V to obtain atomic resolution of the graphite. One set of alkyl chains (row A, Figure 1e) is aligned along a major axis of graphite, and the row direction of the aromatic cores of the aryl-triazoles was found to be oriented at a slight azimuthal angle ($\theta = 10 \pm 2°$) relative to a major axis of graphite (graphite atomic lattice imaged by altering the surface bias to −0.002 V). The inter-alkyl angle is measured to be 100°, so the other set of alkyl chains (row C) are not aligned with a major axis of graphite. The molecular spacing within this array appears to present a reasonable anion-binding pocket, suggesting that the size-matched bromide (Br^-) ion would bind inside, exactly as it does in solution.[45]

Contrary to the expectation that anions will bind directly to this α phase array of receptor cavities, a global phase transition from the α phase to a completely new β phase took place (Figure 1d) in the presence of 1 equiv of Br^- present as the TBA^+ salt. In this case, solutions of **1** and TBABr were mixed before deposition to the HOPG (*ex-situ* mixing) to produce **1**·Br^- complexes in solution (Figure 1b), but the same result is obtained by depositing the solutions sequentially on the surface so that they mix at the solution−solid interface (*in-situ* mixing, Figure S5). The β phase packing model (Figures 1f and S6) is clearly characterized by double rows of aryl-triazoles now arranged head-to-head and with the C_{18} chains aligned along low-index directions of the graphite lattice, allowing interdigitation in a nearly close-packed state (see Section S4 for more detail on alkyl packing in the β phase). The rows of the aromatic cores of the aryl-triazoles are oriented at $30 \pm 3°$ to the low-index direction of the graphite lattice, as indicated in Figure 1f.

This abrupt and obvious repacking of the entire sample surface by receptor **1** is observed only upon anion addition, here with 1 equiv of Br^-. Thus, host−guest complexation between the Br^- and the receptor in solution and at the surface is expected to be critical to the $\alpha \rightarrow \beta$ crystal transformation. Bright features can be observed (Figure 1d, arrow) inside the receptor's binding pocket in the β phase, indicative of the adsorbed complex, **1**·Br^-. Such clearly resolved images of monatomic ions—cationic[23,48−50] or anionic[21]—are rare, particularly for STM imaging in non-UHV environments. A better understanding of the impact of anion binding on this phase transition required appropriate control studies and titration curve measurements, which we now describe.

Anion Binding in Solution. We reasoned that the anion-driven ($\alpha \rightarrow \beta$) phase switching should follow some of the known anion-binding behaviors of this receptor in solution.[45−47,51−54] This class of acyclic[45,47,52,53] aryl-triazole receptors and the related cyclic versions[46,47,51,53,55] have already been thoroughly studied in dichloromethane ($\varepsilon = 9$) solutions with regard to the types of complexes they form, their propensity for ion pairing,[44,45,55] and their binding strengths. This knowledge has accrued from studies that take advantage of quantitative analyses of titration data[44,45,53,55] evaluated with the aid of global analyses and nonlinear regression. These

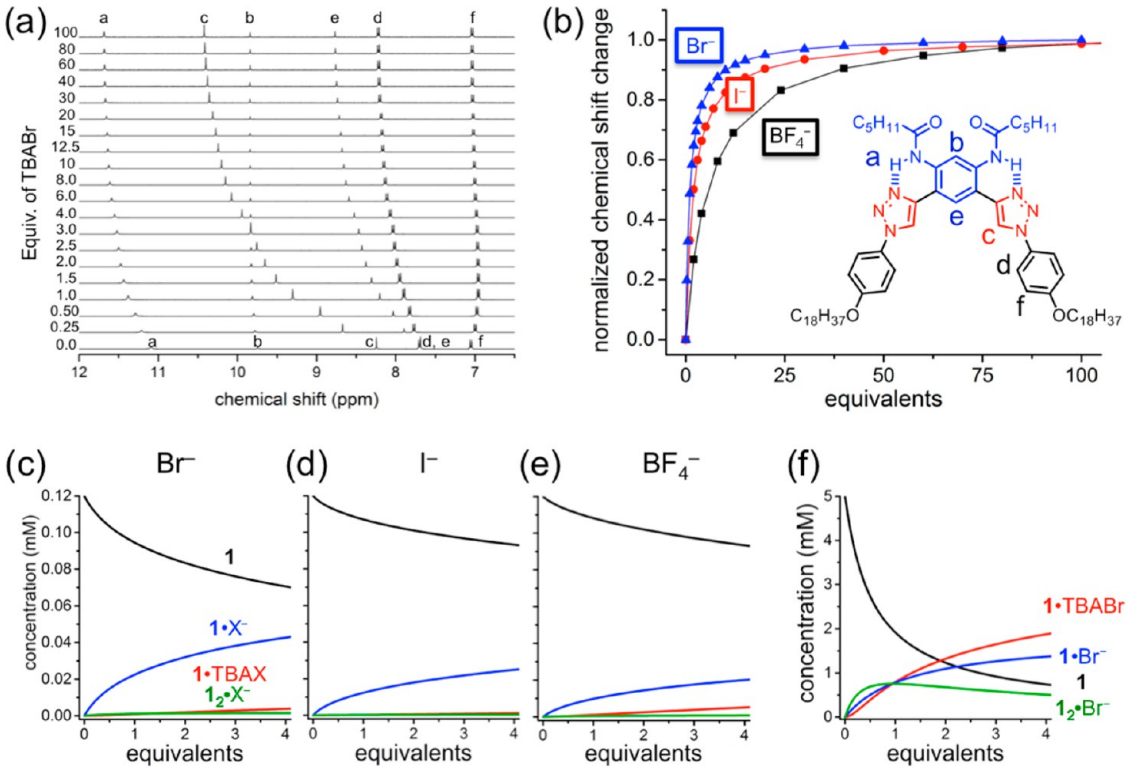

Figure 2. (a) ^{1}H NMR titration data of receptor 1 (5 mM) with TBABr in CD_2Cl_2 with appropriate peak assignments. (b) Titration data following triazole peak H^c as a function of added salt (TBABr, TBAI, TBABF_4). Inset: Labeled chemical structure of receptor 1. Parts (c)−(e) show the speciation curves, which were calculated using the equilibrium constants in Table 1, for the addition of anions (0−5 equiv) to receptor 1 (0.12 mM) corresponding to the STM experiments; (c) TBABr, (d) TBAI, and (e) TBABF_4. (f) Speciation for TBABr added to 1 at NMR concentrations (5 mM).

same approaches were undertaken here with alkyl-functionalized receptor **1**, as exemplified here with Br^-. On the basis of the ^{1}H NMR studies in which TBABr is added to receptor **1** in dichloromethane (Figure 2), we see shifts in peak positions that are indicative of, and provide data for evaluating, the following set of coupled equilibria (see also Figure 3):

$$\mathbf{1} + Br^- \rightleftharpoons \mathbf{1}\cdot Br^- \qquad K_1$$

$$\mathbf{1} + \mathbf{1}\cdot Br^- \rightleftharpoons \mathbf{1}_2\cdot Br^- \qquad K_2$$

$$\mathbf{1}\cdot Br^- + TBA^+ \rightleftharpoons \mathbf{1}\cdot Br^-\cdot TBA^+ \qquad K_{ipc}$$

$$TBA^+ + Br^- \rightleftharpoons TBABr \qquad K_{pair}$$

Here, $\mathbf{1}\cdot Br^-$ is the 1:1 complex (K_1) with the anion sitting in the plane of the receptor's cavity (Figure 3a),[45] $\mathbf{1}_2\cdot Br^-$ is the 2:1 complex (K_2) with the Br^- centrally located between the two receptors coordinated in a distorted tetrahedral geometry[20] (Figure 3b), $\mathbf{1}\cdot Br^-\cdot TBA^+$ is the 1:1:1 ion-paired complex (K_{ipc}) formed between the pre-existing negatively charged complex $\mathbf{1}\cdot Br^-$ and the TBA^+ countercation (Figure 3c),[45,56] and TBABr is the ion pair (Figure 3d) formed in solution when the salt is added to dichloromethane (K_{pair} = 72 000 M^{-1}).[57] The titration analysis of the smooth changes in the ^{1}H NMR peak positions (Figure 2a) is conducted with HypNMR[58]

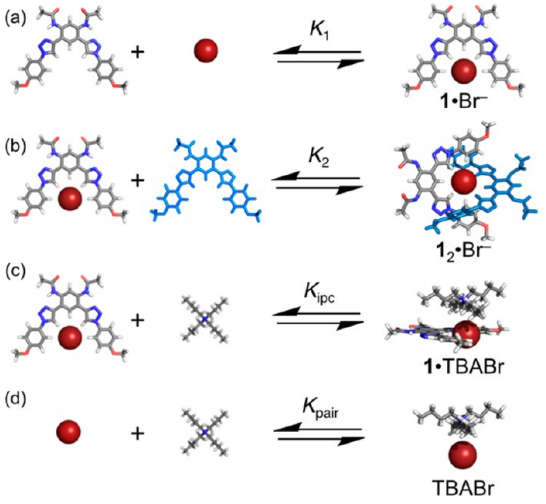

Figure 3. Equilibria present in the solution phase upon addition of Br^- to receptor 1. (a) Formation of the 1:1 complex with geometry-optimized structures (B3LYP/6-31G*). (b) Anion binding with two receptors into a 2:1 complex, showing a methyl-terminated version of a related crystal structure.[59] (c) Formation of the 1:1:1 ion-paired receptor. (d) Ion pairing of the TBA^+ countercation with Br^-. (1 is displayed with the alkyl chains truncated to methyls for clarity of presentation.)

software. The global fitting procedure employs three signals simultaneously, as justified in the following: Proton H^c (Figure 2b) is sensitive to anion binding in the cavity as stabilized by CH···Br^- hydrogen bonding;

TABLE 1. Equilibrium Constants Associated with Binding of Anions to Receptor 1 Obtained from Analysis of ^{1}H NMR Titration Data (CD_2Cl_2)[a]

		X^-		
		Br^-	I^-	BF_4^-
$\mathbf{1}\cdot X^-$	log K_1	3.8 ± 0.4	3.5 ± 0.1	3.5 ± 0.1
$\mathbf{1}_2\cdot X^-$	log K_2	2.7 ± 0.2	2.6 ± 0.3	2.2 ± 0.2
$\mathbf{1}\cdot X^-\cdot TBA^+$	log K_{ipc}	2.8 ± 0.2	3.3 ± 0.2	2.6 ± 0.2
TBAX	log K_{pair}	4.4 ± 0.1[b]	4.4 ± 0.1[b]	4.6 ± 0.2[b]

[a] All anions titrated as TBA^+ salts. Experiments conducted at 5 mM. Global data fitting and error analysis was conducted using HypNMR[58] with protons H^c, H^f, and α-TBA^+. [b] All ion pairing equilibrium values were determined using independent studies by serial dilution and globally fitting the data using energy-restricted factor analysis as enabled with the software Sivvu.[63]

proton H^f is sensitive to formation of the 2:1 complex on account of the fact that it sits inside the face of the aromatic ring of the terminal phenylenes within the bis-receptor complex (Figure 3b); and, the α proton on the TBA^+ countercation is most sensitive to the degree of interaction with the anion on account of the fact that the positive charge is arrayed on these $-CH_2-$ hydrogen atoms.

In addition, the fact that the ^{1}H NMR peaks change position smoothly means that anion binding is dynamic and occurs faster than the NMR time scale. On the basis of the 2 ppm (=800 Hz) difference in peak positions for the free receptor and 1:1 complex, we estimate that the time scale for binding and debinding is less than 0.5 ms in CD_2Cl_2 solution.

The equilibrium constants (Table 1) for binding TBABr, TBAI, and $TBABF_4$ to receptor **1** (eqs 1−4) were established from analysis of the titration data. The titration data show (Figure 2b) that the strength of binding follows the order $Br^- > I^- > BF_4^-$. The change in chemical shift, which correlates with binding strength, is saturated upon addition of fewer equivalents of Br^- than for the other anions. The associated equilibrium constants (Table 1) were then used to calculate the distribution of each complex present upon anion addition using the free software Hyss[60] (Figure 2c−e). These speciation curves show that conversion of the free receptor (**1**) into its various complexed forms ($\mathbf{1}\cdot Br^-$, $\mathbf{1}_2\cdot Br^-$, $\mathbf{1}\cdot$TBABr) follows the same trend as the binding strength. The speciation curve at higher concentrations (Figure 2f), corresponding to the concentration of the ^{1}H NMR data, shows that during the addition of anion to solution there is conversion from one species to the next, and it may be possible to see most of these species including the ion pairing on the surface as an assembly.

Anion-Triggered Crystal Switching. We expect the nature of the crystalline array to modify the binding characteristics of the receptor. For instance, the graphite surface is likely to occlude space and hinder the anions from binding to the cavity in the same geometry as in homogeneous solution. Spatial constraints of the surface adsorption will also affect binding of large anions. In addition, the rigidity conferred upon the receptor by confining it to a 2D crystal may impact its binding properties. For instance, calculations[45] show the crescent shape of the binding pocket can expand to better accommodate larger anions: $d(H^d\cdots H^d)$ for Br^-, I^-, and BF_4^- is 5.6, 5.8, and 6.0 Å (Figure S12). If this induced-fit behavior is hindered within the crystal lattice, then such "rigidity" may manifest as (better or worse) differences in the binding affinities seen in solution. Additionally, complexes with a large deviation from planarity, such as the 2:1 structure (Figure 3b), are not expected to achieve an adsorbed state. Despite all these expectations, the surface stability of each of the ion-bound complexes will be enhanced by the presence of induced charges when the ions are in intimate contact with the conducting HOPG.[61] To aid the comparison to solution values, we also conducted titrations with a 50:50 mix of CD_2Cl_2 with the octanoic acid used for the surface studies. Octanoic acid is found to decrease the extent of anion binding.[62]

There are interesting deviations between solution binding and crystal switching. That is, with 1 equiv added, Br^- completely switches the crystal into the β phase, I^- does so with half the effect, and BF_4^- has no impact. Yet the equilibrium constants for the solution phase binding show modest differences across this series (Table 1). We also conducted experiments with NO_3^- and PF_6^- (Figure S11), which are known to have significantly lower binding constants[64] and do not induce the α → β phase transition. We also note that Cl^-, which binds slightly more tightly than Br^-,[45] does not stabilize the β phase (Figure S10). Selectivity is a behavior usually attributed to rigid and shape-persistent receptors.[54,65] Thus, these data provide hints that the condensation of these receptors into crystalline adlayers may modify the receptor's binding characteristics to increase selectivity. Rigidity is likely to arise when the alkyl chain interdigitation restricts the small in-plane opening and closing of the receptor core. Also, geometry optimizations show (Figure S12) the BF_4^- anion straddles the binding pocket and lowers the receptor's planarity, and such a binding mode might be untenable with the receptor in contact with the surface. The strong affinity of the planar molecule for the surface is likely to limit out-of-plane distortions and may thus exclude the types of binding geometries required for binding BF_4^- (see Figure S12).

The amount of β phase that is produced depends on the amount of anion titrated into the receptor solution (Figure 4c): 1 equiv of Br^- converts the entire surface, whereas 5 equiv of TBAI is needed to achieve a 9:1 β:α mixture. However, these plots (Figure 4c) are not titration curves *per se*. This observation is

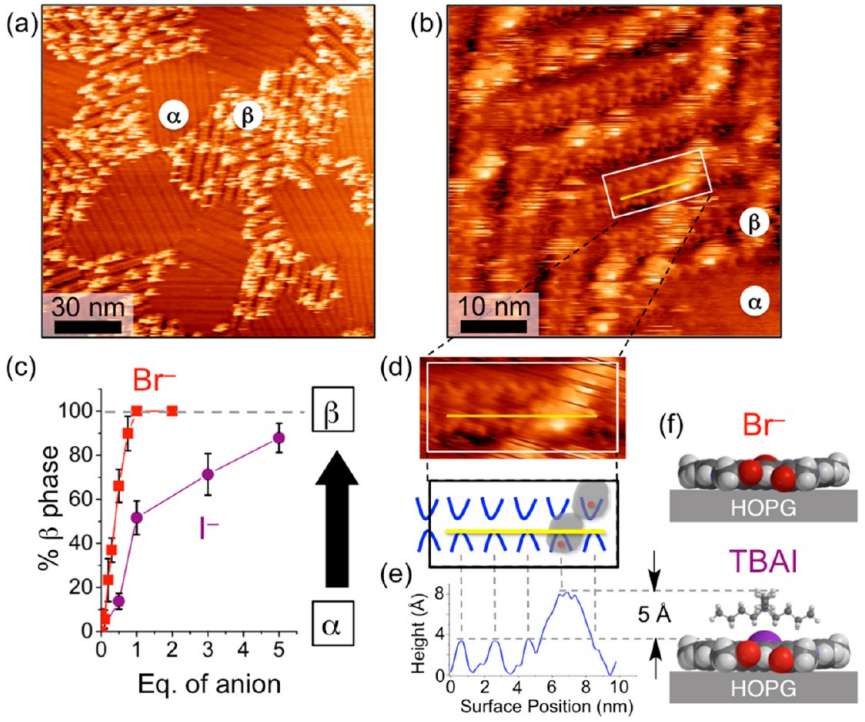

Figure 4. (a, b) STM image of adsorbed 1 in the presence of 1 equiv of TBAI showing a mixed $\alpha-\beta$ phase in (a) a wide scan and (b) a separate scan at greater resolution. (c) Titration plot showing the percentage of surface area covered with the β phase upon addition of varying equivalents of TBABr and TBAI (procedure and estimated error described in the SI). (d) Cropped STM image with schematic model of packing (blue receptors, red I^-, gray TBA^+) and (e) associated line profile (yellow lines). (f) Models of the surface-adsorbed receptors (side view) illustrating the extent of the anion protrusion above the receptor, I^- (purple) and Br^- (red).

consistent qualitatively with the relative strengths of anion binding seen in the solution phase (CD_2Cl_2).[45]

Visualization of Ions and Ion Pairs. Binding site occupancies for Br^- and TBAI in the adsorbate layer of receptors exceed solution behaviors.[45] On the basis of known solution phase binding affinities in CD_2Cl_2 (Figures S15 and S16) and considering that octanoic acid lowers complexation (Figure S17), we expect <10% complexation in the form $\mathbf{1}\cdot Br^-$ (or $\mathbf{1}\cdot I^-$) and ≪1% as $\mathbf{1}\cdot Br^-\cdot TBA^+$ (or $\mathbf{1}\cdot I^-\cdot TBA^+$) in solution at 0.12 mM (1 equiv), as calculated using speciation curves (Figure 2d) for either anion. Yet, binding of TBAI in the β phase as $\mathbf{1}\cdot I^-\cdot TBA^+$ occurs with >90% occupancy when scanning virgin areas (Figure 5a), and ~20% occupation is seen with Br^- (Figure 1a). Unfortunately, even though we see different binding site occupancies between the two anions, these data cannot be used to quantify surface-binding affinities on account of the fact that the same STM tip used for imaging is also responsible for perturbing the system away from equilibrium, *vide infra*.

The halide guests are seen by STM imaging to be dynamic. Some of the bright spots appear (red arrows, Figure 6) and disappear (blue arrows) between sequential images (1 min, see also Figure S13) and even during the time taken to scan from one line to the next (50 ms, green circles). Such half circles are assigned to the desorptive debinding and adsorptive binding of Br^-

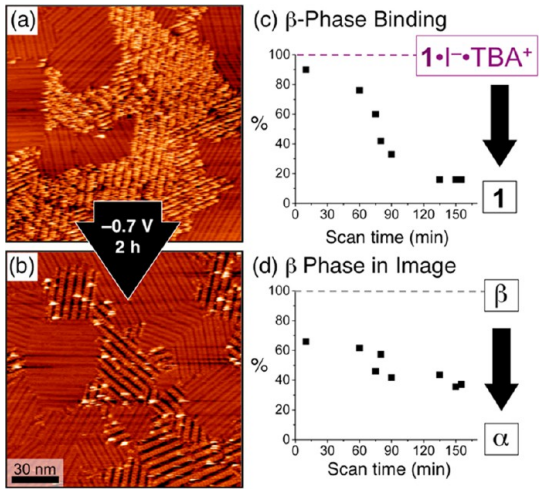

Figure 5. STM images of 1 + 1 equiv of TBAI showing a mixed $\alpha-\beta$ phase at (a) the beginning of repeated scanning at V_{sub} = −0.7 V and (b) after 120 min. (c) Plot of the percentage of adsorbed β phase receptor sites (not counting α sites) occupied by TBAI as a function of scan time. (d) Plot of the percentage of the surface area covered by β phase during the same period of scanning.

and correlate with the rapid dynamics seen in solution (*vide supra*). The same image-to-image (1 min time scale) variation in receptor occupation was observed with I^- (Figure S14). We attribute these observed variations to anion binding and debinding events after excluding several other possibilities: conformational

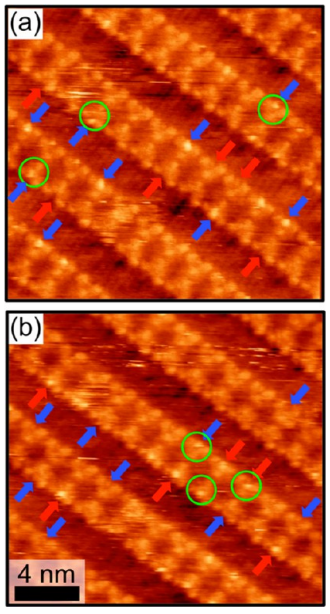

Figure 6. Sequential STM images (Δt = 1 min) showing the dynamic character of the anion binding and debinding from the surface β phase. Images have been corrected for instrument drift and calibrated. Blue arrows indicate nine positions where anions are observed to debind between these two images, while the six red arrows are associated with binding. Green circles highlight six positions where the binding or debinding event is occurring as the tip passes nearby, so that the anion is only partially imaged. Several other binding and debinding events between these images are not marked. For a longer time sequence of images and to see these images without markings, see Figure S13.

changes of the molecule would not produce these features based on the molecule's rigidity and its geometry (Figure 1a), and these features are not observed without anions in the solution, even with the same solvent conditions and STM parameters (Figure 1c).

STM images of the I^--bound complexes in the β phase (Figure 4a, b, d) show additional features sitting ~5 Å above the plane of the complexes that are interpreted to be TBA^+ countercations. Their presence provides evidence of ion-pair complexes within the β phase: $\mathbf{1}\cdot I^-\cdot TBA^+$, analogous to observations of ion pairing between TBA^+ cations and the anion-bound complexes of other aryl-triazole receptors in solution[44,45] and crystal structures.[56]

The extent of ion pairing observed between TBA^+ and the surface-adsorbed complex $\mathbf{1}\cdot I^-$ is greater than expectation from solution behaviors.[45] Herein, we noted that TBA^+ forms an ion pair with the negatively charged complexes $\mathbf{1}\cdot Br^-$ and $\mathbf{1}\cdot I^-$ with low stabilities to form ion-paired complexes, *e.g.*, $\mathbf{1}\cdot I^- + TBA^+ \rightleftharpoons \mathbf{1}\cdot I^-\cdot TBA^+$, K_{ipc} ~4000 M^{-1} (CD_2Cl_2) (see Table 1). There is more frequent observation of ion pairing with I^- than with Br^-, which we attribute to modification of the ion pairing behavior upon adsorption of the receptor–anion complex. A plausible explanation for this change is that $\mathbf{1}\cdot I^-$ complexes in the adsorbed β phase display a greater charge density in solution than does $\mathbf{1}\cdot Br^-$. Such a situation would allow for more stable Coulombic contacts with the TBA^+ cation. But, general expectations derived from solution studies[44,45] suggest that the more charge-dense Br^- should pair more than I^-, which is the opposite of what we observe for the surface-confined situation. To rationalize the observation, we again consider the impact of the crystalline adlayer and the sizes of the constituent atoms $I^- > Br^- > C$ (diameters: d_{I^-} = 4.4 Å, d_{Br^-} = 3.8 Å, d_C = 3.4 Å). Thus, assuming the anions and the receptors are reasonably flat-lying on the surface, the significantly larger size of I^- may allow as much as ~1 Å of this anion to be sitting (Figure 4f) in a dome-like manner out of the receptor's cavity and into the solution, while only 0.4 Å of the Br^- will be exposed. This size difference allows I^- to display three times more surface area in solution than Br^-, causing greater ion pairing. This effect can be interpreted in two ways. First, in collisional ion pair formation, a larger surface area will lead statistically to more ion pairs being formed. Second, the exposed iodide may present a larger surface on which the cation, with its positive charge known to localize on the $-CH_2-$ hydrogens, can interact. The observation of behavior that deviates from the solution phase lends further support to the idea that confinement of the receptor to an interfacial crystalline array modifies its binding properties in unanticipated ways.

Thermal Activation of Anion Binding. Reversible anion binding within the β phase should render the assembly susceptible to thermal debinding. According to our interpretation of the interactions stabilizing each phase, thermally activated anion debinding should destabilize the β phase and cause phase switching back to the ion-free α phase globally. Experiments were conducted by acquiring STM images between incremental increases in the temperature of the HOPG sample. On the basis of the STM imaging, the $\beta \rightarrow \alpha$ transitions seem to be abrupt and global: with the sample at 56 °C (Figure 7b) the sample is still covered by the β phase. In the next STM image with the sample now at 57 °C (Figure 7c), the surface is completely populated by the α phase; the structure observed here is equivalent to images recorded at similar scan sizes for samples without anion present. With 1 equiv of TBAI, the steady-state monolayer at room temperature is a 50:50 α:β mixture (Figure 7e). We did not observe any significant change in surface structure up to 29 °C (Figure 7f), but then in the subsequent image at 30 °C (Figure 7g), the entire surface had transitioned to α phase. The lower transition temperature for I^- correlates with its weaker stabilization of the β phase. With either TBABr or TBAI, the room-temperature steady-state structure is restored upon cooling (Figure 7d and h).

Response to STM Electric Field. Contrary to all prior ion-triggered phase transitions, we were surprised to observe that the TBAI-bound β phase structure (Figure 8a)

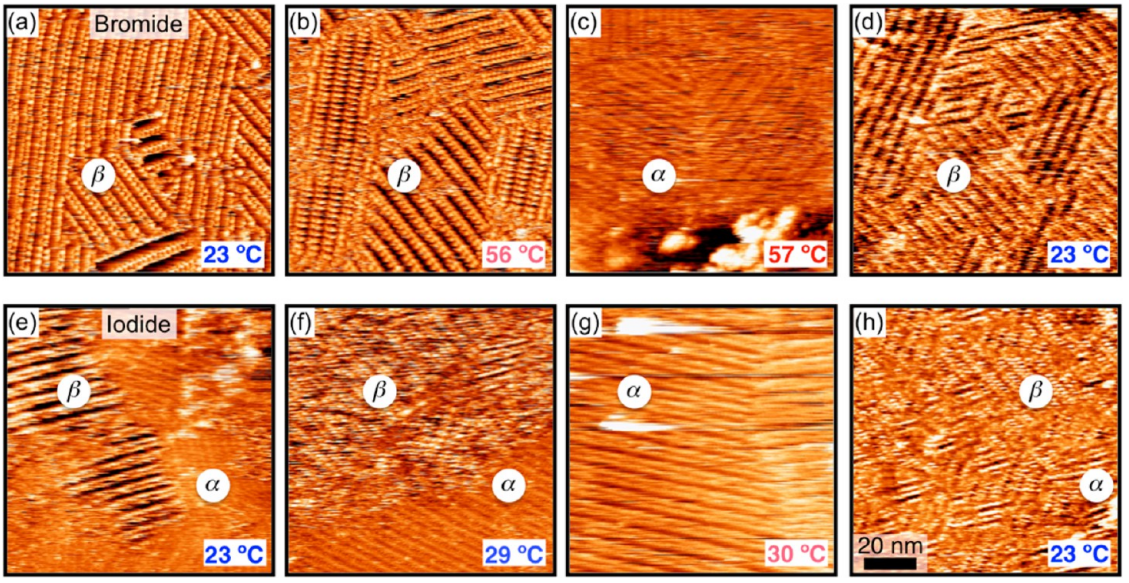

Figure 7. STM images showing temperature-dependent phase transitions of 1 (0.12 mM) with (a–d) 1 equiv of TBABr occurring at 57 °C and (e–h) 1 equiv of of TBAI at 30 °C. α and β phases are labeled. Scale bar is the same for each of the panels. (V_{sub} = −0.7 V, I_T = 10 pA.)

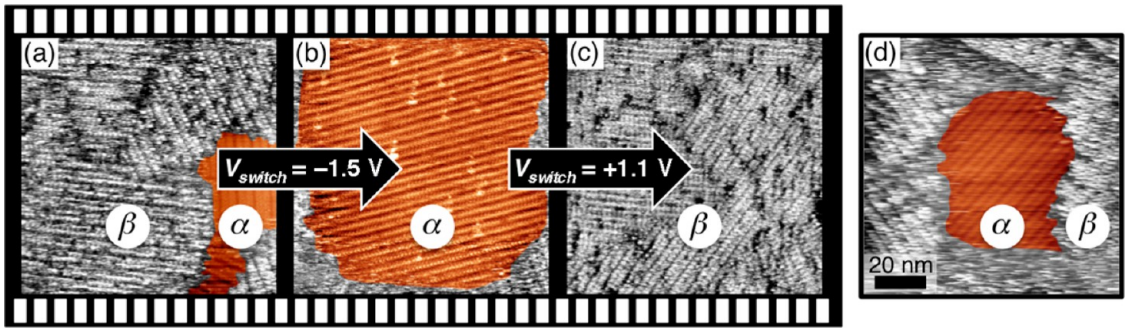

Figure 8. (a) Initial STM image of the β phase (gray tint) obtained from a solution of 1 + TBAI (octanoic acid, V_{sub} = −0.7 V, [1] = [I^-] = 1.2 × 10^{-4} M^{-1}). The larger (b) negative (−1.5 V) then (c) positive (+1.1 V) biases drive switching between the anion-bound β phase and the uncomplexed α phase, respectively. Time sequence of the voltage-induced phase switching is available as Supporting Information (Movie S1 and Figure S19). (d) Separate experiment showing localization of switching effect after "writing" the α phase crystal structure into a smaller region (prior "writing" scan was at −1.5 V bias in a 20 nm × 20 nm region). All four images are 100 nm × 100 nm in size and were recorded with I_T = 10 pA and V_{sub} = (a, c, d) −0.7 V or (b) −1.5 V.

could be transformed locally into the α phase (orange tint, Figure 8b) by scanning for ∼10 min with a substrate voltage (V_{sub}) of −1.5 V. This switching was found to be reversible (Figure 8c) by scanning at +1.1 V for ∼10 min (Figure S19, movie S1). A substrate voltage of −0.7 V was used to generate molecular resolution in Figure 7c; the β phase lamella spacing is imaged at +1.1 V (Figure S20), but molecular resolution was not achieved. Switching the voltage from +1.1 to −0.7 V part way through the image unambiguously reveals the β phase (Figure S20). As can be seen in a time sequence of images (Figure S19), this local switching effect begins immediately upon changing bias, but takes several scans (over several minutes) in order to form a highly ordered region of the new phase. The relatively slow switching here compared to thermal activation is likely due to the spatially confined nature of the strongest region of the electric field. Switching is a local effect corresponding to the surface region over which the STM tip is scanning, as shown by the zoom-out image in Figure 8d. Thus, one can use the STM tip to cycle between the global equilibrium β phase and a localized, nonequilibrium α phase.

There are many examples of local tip-induced transitions or transformations. Of the two prior examples of such transitions using an *E*-field,[36,37] one shows programmable switching with the *E*-field but only produces an order–disorder transition.[37] The other does not follow the logical response expected of a charge in an *E*-field and thus does not exhibit polarity-dependent programming of the transition.[36] For this reason, we conducted a series of control experiments to better characterize the origin of the programmable order–order transition seen in the present supramolecular assembly.

Anions are required for switching; the *E*-field (in either polarity) has no effect on the observed phase

distribution without them; see Figure S21. The −1.5 V bias is believed to activate decomplexation of the anions, thereby destabilizing the β phase and allowing the α phase to form. By the same logic, +1.1 V enriches the anions at the surface and leads expediently to re-formation of the anion-stabilized β phase. Note that the equilibrium β phase will also re-form with no bias applied at the surface, but that the −0.7 V "imaging bias" slows β regrowth substantially.

Persistent scanning using less negative biases over the same area also drives switching (Figure 5). Repeated scanning of a TBAI-dosed sample (1 equiv) at −0.7 V for over 2 h (Figure 5b) shows extensive loss of TBAI from the β phase (90% → 15% occupancy, Figure 5c) and a modest degree of switching into the α phase (35% → 55%, Figure 5d). These data suggest that the rate of these particular dynamics (among others) differs between high and low tip biases. The actual occupancy of the surface-adsorbed receptors in virgin areas unperturbed by the scanning tip is expected to be equal to or higher than those observed by STM.

E-fields drive switching of this system. Consistent with this idea, we have observed that the response depends on the polarity and magnitude of the field. We do not believe that proximity between the sample and the tip can drive switching because lower voltages (−0.7 V), which bring the tip closer to the adlayer, slow switching (Figure 5) instead of hastening it. If the effect originated from inelastic tunneling (excitation of molecular vibrations), it should turn on at a lower voltage (less than about 370 mV ≡ 3000 cm^{-1}). Our observations follow the logic of how a charged anion should respond to an *E*-field, the direct interaction of the anion with the local *E*-field (on the order of 10^9 V m^{-1}) is very significant, the $\beta \leftrightarrows \alpha$ switching correlates with *E*-field polarity, and $\alpha \rightarrow \beta$ switching occurs only at +1.1 V if the anions are present (Figure S21).

Crystal switching of **1**·Br^- appears to be more difficult than with **1**·I^-, requiring either lower concentrations of Br^- or higher switching biases. At −0.7 V substrate bias, the switch occurs only with substoichiometric Br^-, a situation that ensures some α phase is present at the surface and suggests that seeding of the α phase growth might be important. At 0.2 equiv of Br^-, the β phase can be switched to α by imaging at −0.7 V over ~30 min (Figure S22). With 1 equiv of Br^-, a more negative substrate bias is required to induce switching to α phase: complete loss of the β phase locally is observed within two scans at −1.8 V (Figure S23).

As discussed above, the Br^- anion shows low anion occupancy within the β phase receptors. The low Br^- occupancy is likely due to the bromide's sensitivity to the scanning E-field. By comparison, TBAI is seen with high occupancies and almost exclusively as the ion pair. As such, we can view the ion pair as a dipolar zwitterion that will couple differently to *E*-fields. It is for these reasons that we believe the surface-bound

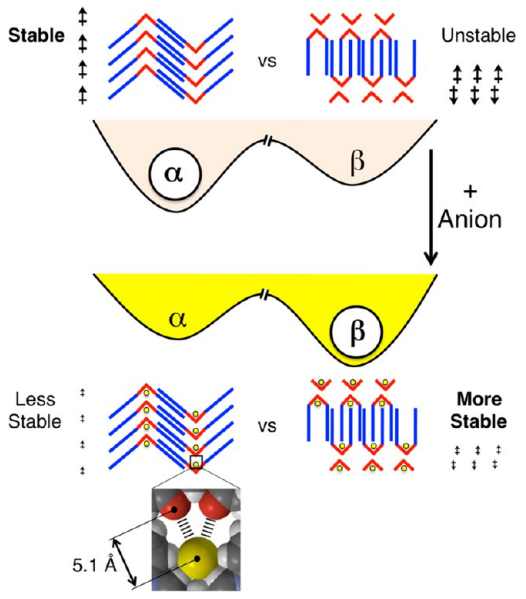

Figure 9. Models showing the principle anion-driven changes in dipole coupling and local electrostatic contacts that lead to reversible and bistable switching between α and β phases. Cartoons of the molecules are represented by red cores and blue tails. The space fill model showing close-contact repulsions is based on the spacing present in the 2D crystal structure solution.

complexes formed with TBAI are more stable near the scanning probe than the Br^- complexes.

Summary. Interestingly, this self-assembled system is responsive and bistable despite the fact that the molecule is not programmed to change its shape upon anion binding. There are several factors that contribute to this behavior, which we now discuss. First, while the alkyl chains exist in different arrangements in the two phases ($\alpha \equiv$ out−out, 100°, $\beta \equiv$ in−in, parallel), the energy differences between the conformations (B3LYP/6-31G*) are modest irrespective of whether the anion is bound or not (Figure S9). Second, the experimentally observed unit cells indicate that, with regard to vdW interactions, there exists an energetic advantage of the β phase that results from greater vdW contacts of the receptors' alkyls with the surface and their nearest neighbors. That is, neither the adsorbate's conformations nor the vdW contacts are affected by anion binding, and for this reason, we do not believe they contribute to the switching between α and β phases.

The role of the anion must be considered in the switching behavior. An examination of the packing structure and of the constituent molecules allows an evaluation of the attractive and repulsive contacts that will contribute to the relative stabilities of the phases. The third factor, therefore, is the existence of repulsive clashes[66] arising from local electrostatic contacts between an anion bound to one receptor and the proximal carbonyl oxygens on the neighboring receptor (Figure 9). These contacts will be present in the α phase

and act to destabilize it, but similar ion−dipole type contacts are absent in the β phase. Fourth, we consider that the large molecular dipole from the receptor will have an impact. For the neutral receptor, we calculated a 16 D dipole for the out−out conformation present in the α phase and a 19 D dipole for the in−in conformation in the β phase. The α phase will be stabilized by the head-to-tail coupling of the 16 D dipoles, and by contrast, the β phase will be destabilized by the head-to-head clashes from the 19 D dipoles. Our calculations show that the dipoles are more than halved upon anion binding; out−out $\alpha \equiv 6$ D and in−in $\beta \equiv 9$ D. Thus, the positive and negative impact of longer range dipole−dipole coupling will be lessened between the two phases upon anion binding. Consequently, anion binding is believed to invert the relative stabilities of the two phases by altering the combination of forces that only emerge at the level of the crystal. This leads to a qualitative understanding of switching: Anion binding (1) weakens the stability of the α phase by local anion-to-carbonyl electrostatic clashes and (2) lowers the energy differences between the two phases that originate from dipole coupling. We believe these two effects modify the thermodynamic landscape of the system to destabilize the α phase and increase the stability of the β phase upon anion binding (Figure 9). Once the β phase is formed, it provides a binding site for the anion (Figure 6) or ion pair (Figure 4b). When the *E*-field from the tip stimulates ion release from a surface-adsorbed receptor, the phase stability flips back from the β to the α.

We have also shown that the behaviors of the receptors, when confined at the solution−graphite interface and in a crystalline array, differ from their solution phase behaviors. The crystal switching displayed a selective response to only Br^- and I^- even though in solution these two anions are merely members of a homologous series that show the following trend in their binding affinities (Table 1): $Cl^- > Br^- > I^- > BF_4^-$. In the observations of enhanced ion pairing for I^-, we observed behavior that is the opposite of that seen in homogeneous solutions. These observations indicate that the interfacial and rigid character of the 2D crystal changes the receptor's sensitivity to different anions. We note that these types of observations have benefitted from varying the anions added, varying the amounts of each anion added, optimizing the parameters needed to visualize the anions and ion pairs, and the fortuitous switch in crystal morphology. There is every reason to believe that these types of effects are present in other ion-binding arrays.

CONCLUSION

This work presents an exemplary supramolecular host−guest system for probing how solution phase behaviors originating from host−guest chemistry can be affected by surface adsorption: some properties remain the same (anion binding), others change (anion selectivity), while still others are completely new, such as phase switching and *E*-field responsivity. A global anion-induced phase switching at the surface is a consequence of the hierarchical ordering present in the 2D self-assembled crystalline material. We demonstrate how the reversible and selective binding of anions to adsorbed receptors sensitized the 2D monolayer to *E*-field-driven crystal switching by the scanning probe. High-resolution STM imaging provides molecular-level insight into anion-binding events, supramolecular phase switching, and ion pairing effects within the adsorbed monolayer at the solution−solid interface. Comparisons of anion-binding behaviors at the interface with detailed titration analyses in solution demonstrate that anion selectivity is strongly affected by self-assembly into crystalline monolayers at the surface. The broader implication of this study is that the functionality of small molecules, such as guest recognition and environmental response, can be dramatically impacted when the molecules are ordered into condensed phases.

EXPERIMENTAL SECTION

Scanning tunneling microscopy experiments were carried out on Agilent Technologies 5500 PicoPlus STM using a Picoscan controller in constant-current mode. Tips were mechanically cut from Pt/Ir wire (80:20, diameter 0.2 mm). The HOPG substrate (ZYB, Mikromasch or Structure Probe, Inc.) was mechanically cleaved before each experiment.

A liquid cell was made from Teflon using a Viton O-ring to ensure the surface area was consistent between experiments. Samples were prepared by dropping 10 μL of solution on the surface with a microsyringe. Solutions of aryl-triazole receptor **1** were prepared in octanoic acid (≥98%, Aldrich) across a range of concentrations (1 μM to 1 mM). Solutions of the anions were prepared from the corresponding tetrabutylammonium salts in octanoic acid and were added to the aryl-triazole solution in either an *ex-situ* or *in-situ* manner. *Ex-situ* mixing was performed by premixing the receptor and anion solutions before deposition. *In-situ* mixing was performed by withdrawing the tip after confirming formation of the free receptor assembly, followed by addition of anion solution with a microsyringe.

Variable-temperature experiments were conducted using a heater built into the sample support plate, which was controlled with a LakeShore 331 controller with a type K thermocouple. The setup is capable of controlling the temperature of the sample surface to better than ±0.05 °C. Surface coverage fraction (χ) of the α and β phases was determined as an average based on more than three experiments (new surface cleavage). The relative coverage was determined by using more than 20 images (100 nm × 100 nm) obtained in different areas (separated by ~5 μm) across the surface. All high-resolution STM images were corrected for drift effects and piezo scanner calibration by comparison to lattice measurements of the underlying HOPG (recorded using scan conditions different from those used to measure molecular assemblies, $I_t = 0.1$ nA, $V_{bias} = -0.002$ V). Unit cell measurements (including angles relative to the HOPG lattice) were acquired after correcting the high-resolution images and averaging the distances.

Conflict of Interest: The authors declare no competing financial interest.

Supporting Information Available: Molecular and crystal models; anion and voltage switching STM data; anion binding; movie; syntheses. This material is available free of charge *via* the Internet at http://pubs.acs.org.

Acknowledgment. B.E.H. acknowledges support from Indiana University and the Strawn Fellowship. K.P.M. acknowledges Indiana University and the Paget Organic Fellowship. S.L.T. acknowledges funding for the STM instrument from the METACyt Initiative, Indiana University. A.H.F. acknowledges support from Indiana University and the Dreyfus Foundation.

REFERENCES AND NOTES

1. Aida, T.; Meijer, E. W.; Stupp, S. I. Functional Supramolecular Polymers. *Science* **2012**, *335*, 813–817.
2. De Feyter, S.; Gesquière, A.; Abdel-Mottaleb, M. M.; Grim, P. C. M.; De Schryver, F. C.; Meiners, C.; Sieffert, M.; Valiyaveettil, S.; Müllen, K. Scanning Tunneling Microscopy: A Unique Tool in the Study of Chirality, Dynamics, and Reactivity in Physisorbed Organic Monolayers. *Acc. Chem. Res.* **2000**, *33*, 520–531.
3. Mali, K. S.; Adisoejoso, J.; Ghijsens, E.; De Cat, I.; De Feyter, S. Exploring the Complexity of Supramolecular Interactions for Patterning at the Liquid-Solid Interface. *Acc. Chem. Res.* **2012**, *45*, 1309–1320.
4. Schull, G.; Douillard, L.; Fiorini-Debuisschert, C.; Charra, F.; Mathevet, F.; Kreher, D.; Attias, A. J. Selectivity of Single-Molecule Dynamics in 2D Molecular Sieves. *Adv. Mater.* **2006**, *18*, 2954–2957.
5. Lei, S. B.; Tahara, K.; Feng, X. L.; Furukawa, S. H.; De Schryver, F. C.; Müllen, K.; Tobe, Y.; De Feyter, S. Molecular Clusters in Two-Dimensional Surface-Confined Nanoporous Molecular Networks: Structure, Rigidity, and Dynamics. *J. Am. Chem. Soc.* **2008**, *130*, 7119–7129.
6. Abdel-Mottaleb, M. M. S.; Schuurmans, N.; De Feyter, S.; Van Esch, J.; Feringa, B. L.; De Schryver, F. C. Submolecular Visualisation of Palladium Acetate Complexation with a Bipyridine Derivative at a Graphite Surface. *Chem. Commun.* **2002**, 1894–1895.
7. Surin, M.; Samori, P.; Jouaiti, A.; Kyritsakas, N.; Hosseini, M. W. Molecular Tectonics on Surfaces: Bottom-Up Fabrication of 1D Coordination Networks that Form 1D and 2D Arrays on Graphite. *Angew. Chem., Int. Ed.* **2007**, *46*, 245–249.
8. Ciesielski, A.; Piot, L.; Samori, P.; Jouaiti, A.; Hosseini, M. W. Molecular Tectonics at the Solid/Liquid Interface: Controlling the Nanoscale Geometry, Directionality, and Packing of 1D Coordination Networks on Graphite Surfaces. *Adv. Mater.* **2009**, *21*, 1131–1136.
9. Piot, L.; Meudtner, R. M.; El Malah, T.; Hecht, S.; Samorì, P. Modulating Large-Area Self-Assembly at the Solid−Liquid Interface by pH-Mediated Conformational Switching. *Chem.—Eur. J.* **2009**, *15*, 4788–4792.
10. Zell, P.; Mogele, F.; Ziener, U.; Rieger, B. Fine-Tuning of Relative Metal-Metal Distances within Highly Ordered Chiral 2D Nanopatterns. *Chem.—Eur. J.* **2006**, *12*, 3847–3857.
11. Ciesielski, A.; Lena, S.; Masiero, S.; Spada, G. P.; Samorì, P. Dynamers at the Solid−Liquid Interface: Controlling the Reversible Assembly/Reassembly Process between Two Highly Ordered Supramolecular Guanine Motifs. *Angew. Chem., Int. Ed.* **2010**, *49*, 1963–1966.
12. Gutzler, R.; Sirtl, T.; Dienstmaier, J. F.; Mahata, K.; Heckl, W. M.; Schmittel, M.; Lackinger, M. Reversible Phase Transitions in Self-Assembled Monolayers at the Liquid-Solid Interface: Temperature-Controlled Opening and Closing of Nanopores. *J. Am. Chem. Soc.* **2010**, *132*, 5084–5090.
13. Lee, S.-L.; Yuan, Z.; Chen, L.; Mali, K. S.; Müllen, K.; De Feyter, S. Forced to Align: Flow-Induced Long-Range Alignment of Hierarchical Molecular Assemblies from 2D to 3D. *J. Am. Chem. Soc.* **2014**, *136*, 4117–4120.
14. Tahara, K.; Inukai, K.; Adisoejoso, J.; Yamaga, H.; Balandina, T.; Blunt, M. O.; De Feyter, S.; Tobe, Y. Tailoring Surface-Confined Nanopores with Photoresponsive Groups. *Angew. Chem., Int. Ed.* **2013**, *52*, 8373–8376.
15. Bleger, D.; Ciesielski, A.; Samori, P.; Hecht, S. Photoswitching Vertically Oriented Azobenzene Self-Assembled Monolayers at the Solid-Liquid Interface. *Chem.—Eur. J.* **2010**, *16*, 14256–14260.
16. Sessler, J. L.; Gale, P. A.; Cho, W. S. *Anion Receptor Chemistry*; RSC: London, 2006.
17. Nelson, D. L.; Lehninger, A. L.; Cox, M. M. *Lehninger Principles of Biochemistry*, 5 ed.; W. H. Freeman: New York, 2008.
18. Fahim, M. A.; Alsahhaf, T. A.; Elkilani, A. *Fundamentals of Petroleum Refining*; Elsevier: Oxford, 2010.
19. Maeda, H.; Shirai, T.; Uemura, S. Anion-Driven Structures of Radially Arranged Anion Receptor Oligomers. *Chem. Commun.* **2013**, *49*, 5310–5312.
20. Hirsch, B. E.; Lee, S.; Qiao, B.; Chen, C.-H.; McDonald, K. P.; Tait, S. L.; Flood, A. H. Anion-Induced Dimerization of 5-Fold Symmetric Cyanostars in 3D Crystalline Solids and 2D Self-Assembled Crystals. *Chem. Commun.* **2014**, *50*, 9827–9830.
21. Kudernac, T.; Shabelina, N.; Mamdouh, W.; Hoger, S.; De Feyter, S. STM Visualisation of Counterions and the Effect of Charges on Self-Assembled Monolayers of Macrocycles. *Beilstein J. Nanotechnol.* **2011**, *2*, 674–680.
22. Steed, J. W.; Atwood, J. L. Anion Binding. In *Supramolecular Chemistry*; John Wiley & Sons, Ltd, 2009; pp 223−284.
23. Skomski, D.; Abb, S.; Tait, S. L. Robust Surface Nano-Architecture by Alkali-Carboxylate Ionic Bonding. *J. Am. Chem. Soc.* **2012**, *134*, 14165–14171.
24. Skomski, D.; Tait, S. L. Ordered and Robust Ionic Surface Networks from Weakly Interacting Carboxyl Building Blocks. *J. Phys. Chem. C* **2013**, *117*, 2959–2965.
25. Wan, L. J.; Noda, H.; Wang, C.; Bai, C. L.; Osawa, M. Controlled Orientation of Individual Molecules by Electrode Potentials. *ChemPhysChem* **2001**, *2*, 617–619.
26. Su, G. J.; Zhang, H. M.; Wan, L. J.; Bai, C. L. Phase Transition of Thiophene Molecules on Au(111) in Solution. *Surf. Sci.* **2003**, *531*, 363–368.
27. Baunach, T.; Ivanova, V.; Scherson, D. A.; Kolb, D. A. Self-Assembled Monolayers of 4-Mercaptopyridine on Au(111): A Potential-Induced Phase Transition in Sulfuric Acid Solutions. *Langmuir* **2004**, *20*, 2797–2802.
28. Su, G. J.; Zhang, H. M.; Wan, L. J.; Bai, C. L.; Wandlowski, T. Potential-Induced Phase Transition of Trimesic Acid Adlayer on Au(111). *J. Phys. Chem. B* **2004**, *108*, 1931–1937.
29. Yoshimoto, S.; Tada, A. K.; Suto, K.; Yau, S. L.; Itaya, K. *In Situ* Scanning Tunneling Microscopy of Molecular Assemblies of Cobalt(II)- and Copper(II)-Coordinated Tetraphenyl Porphine and Phthalocyanine on Au(100). *Langmuir* **2004**, *20*, 3159–3165.
30. Li, Z.; Han, B.; Wan, L. J.; Wandlowski, T. Supramolecular Nanostructures of 1,3,5-Benzene-Tricarboxylic Acid at Electrified Au(111)/0.05 M H_2SO_4 Interfaces: An *In Situ* Scanning Tunneling Microscopy Study. *Langmuir* **2005**, *21*, 6915–6928.
31. Zhang, J. D.; Demetriou, A.; Welinder, A. C.; Albrecht, T.; Nichols, R. J.; Ulstrup, J. Potential-Induced Structural Transitions of DL-Homocysteine Monolayers on Au(111) Electrode Surfaces. *Chem. Phys.* **2005**, *319*, 210–221.
32. Klymchenko, A. S.; Furukawa, S.; Müllen, K.; Van der Auweraer, M.; De Feyter, S. Supramolecular Hydrophobic-Hydrophilic Nanopatterns at Electrified Interfaces. *Nano Lett.* **2007**, *7*, 791–795.
33. Klymchenko, A. S.; Furukawa, S.; Van der Auweraer, M.; Müllen, K.; De Feyter, S. Directing the Assembly of Charged Organic Molecules by a Hydrophilic-Hydrophobic Nanostructured Monolayer at Electrified Interfaces. *Nano Lett.* **2008**, *8*, 1163–1168.
34. Su, G. J.; Li, Z. H.; Aguilar-Sanchez, R. Phase Transition of Two-Dimensional Chiral Supramolecular Nanostructure Tuned by Electrochemical Potential. *Anal. Chem.* **2009**, *81*, 8741–8748.

35. Cui, K.; Ivasenko, O.; Mali, K. S.; Wu, D.; Feng, X.; Müllen, K.; De Feyter, S.; Mertens, S. F. L. Potential-Driven Molecular Tiling of a Charged Polycyclic Aromatic Compound. *Chem. Commun.* **2014**, *50*, 10376–10378.
36. Mali, K. S.; Wu, D.; Feng, X.; Müllen, K.; Van der Auweraer, M.; De Feyter, S. Scanning Tunneling Microscopy-Induced Reversible Phase Transformation in the Two-Dimensional Crystal of a Positively Charged Discotic Polycyclic Aromatic Hydrocarbon. *J. Am. Chem. Soc.* **2011**, *133*, 5686–5688.
37. Lei, S.-B.; Deng, K.; Yang, Y.-L.; Zeng, Q.-D.; Wang, C.; Jiang, J.-Z. Electric Driven Molecular Switching of Asymmetric Tris(Phthalocyaninato) Lutetium Triple-Decker Complex at the Liquid/Solid Interface. *Nano Lett.* **2008**, *8*, 1836–1843.
38. Semenov, A.; Spatz, J. P.; Möller, M.; Lehn, J. M.; Sell, B.; Schubert, D.; Weidl, C. H.; Schubert, U. S. Controlled Arrangement of Supramolecular Metal Coordination Arrays on Surfaces. *Angew. Chem., Int. Ed.* **1999**, *38*, 2547–2550.
39. Safarowsky, C.; Merz, L.; Rang, A.; Broekmann, P.; Hermann, B. A.; Schalley, C. A. Second-Order Templation: Ordered Deposition of Supramolecular Squares on a Chloride-Covered Cu(100) Surface. *Angew. Chem., Int. Ed.* **2004**, *43*, 1291–1294.
40. Yuan, Q. H.; Wan, L. J.; Jude, H.; Stang, P. J. Self-Organization of a Self-Assembled Supramolecular Rectangle, Square, and Three-Dimensional Cage on Au(111) Surfaces. *J. Am. Chem. Soc.* **2005**, *127*, 16279–16286.
41. Gong, J. R.; Wan, L. J.; Yuan, Q. H.; Bai, C. L.; Jude, H.; Stang, P. J. Mesoscopic Self-Organization of a Self-Assembled Supramolecular Rectangle on Highly Oriented Pyrolytic Graphite and Au(111) Surfaces. *Proc. Natl. Acad. Sci. U.S.A.* **2005**, *102*, 971–974.
42. Yuan, Q. H.; Yan, C. J.; Yan, H. J.; Wan, L. J.; Northrop, B. H.; Jude, H.; Stang, P. J. Scanning Tunneling Microscopy Investigation of a Supramolecular Self-Assembled Three-Dimensional Chiral Prism on a Au(111) Surface. *J. Am. Chem. Soc.* **2008**, *130*, 8878–8879.
43. Li, S.-S.; Yan, H.-J.; Wan, L.-J.; Yang, H.-B.; Northrop, B. H.; Stang, P. J. Control of Supramolecular Rectangle Self-Assembly with a Molecular Template. *J. Am. Chem. Soc.* **2007**, *129*, 9268–9269.
44. Hua, Y.; Ramabhadran, R. O.; Uduehi, E. O.; Karty, J. A.; Raghavachari, K.; Flood, A. H. Aromatic and Aliphatic CH Hydrogen Bonds Fight for Chloride While Competing Alongside Ion Pairing within Triazolophanes. *Chem.—Eur. J.* **2011**, *17*, 312–321.
45. McDonald, K. P.; Ramabhadran, R. O.; Lee, S.; Raghavachari, K.; Flood, A. H. Polarized Naphthalimide CH Donors Enhance Cl^- Binding within an Aryl-Triazole Receptor. *Org. Lett.* **2011**, *13*, 6260–6263.
46. Li, Y.; Flood, A. H. Pure C-H Hydrogen Bonding to Chloride Ions: A Preorganized and Rigid Macrocyclic Receptor. *Angew. Chem., Int. Ed.* **2008**, *47*, 2649–2652.
47. Hua, Y.; Flood, A. H. Click Chemistry Generates Privileged CH Hydrogen-Bonding Triazoles: The Latest Addition to Anion Supramolecular Chemistry. *Chem. Soc. Rev.* **2010**, *39*, 1262–1271.
48. Lin, N.; Dmitriev, A.; Weckesser, J.; Barth, J. V.; Kern, K. Real-Time Single-Molecule Imaging of the Formation and Dynamics of Coordination Compounds. *Angew. Chem., Int. Ed.* **2002**, *41*, 4779–4783.
49. Messina, P.; Dmitriev, A.; Lin, N.; Spillmann, H.; Abel, M.; Barth, J. V.; Kern, K. Direct Observation of Chiral Metal-Organic Complexes Assembled on a Cu(100) Surface. *J. Am. Chem. Soc.* **2002**, *124*, 14000–14001.
50. Spillmann, H.; Dmitriev, A.; Lin, N.; Messina, P.; Barth, J. V.; Kern, K. Hierarchical Assembly of Two-Dimensional Homochiral Nanocavity Arrays. *J. Am. Chem. Soc.* **2003**, *125*, 10725–10728.
51. Li, Y.; Vander Griend, D. A.; Flood, A. H. Modelling Triazolophane−Halide Binding Equilibria Using Sivvu Analysis of UV−Vis Titration Data Recorded under Medium Binding Conditions. *Supramol. Chem.* **2009**, *21*, 111–117.
52. Lee, S.; Hua, Y.; Park, H.; Flood, A. H. Intramolecular Hydrogen Bonds Preorganize an Aryl-Triazole Receptor into a Crescent for Chloride Binding. *Org. Lett.* **2010**, *12*, 2100–2102.
53. McDonald, K. P.; Hua, Y.; Lee, S.; Flood, A. H. Shape Persistence Delivers Lock-and-Key Chloride Binding in Triazolophanes. *Chem. Commun.* **2012**, *48*, 5065–5075.
54. Lee, S.; Chen, C. H.; Flood, A. H. A Pentagonal Cyanostar Macrocycle with Cyanostilbene CH Donors Binds Anions and Forms Dialkylphosphate [3]Rotaxanes. *Nat. Chem.* **2013**, *5*, 704–710.
55. Ramabhadran, R. O.; Liu, Y.; Hua, Y.; Ciardi, M.; Flood, A. H.; Raghavachari, K. An Overlooked yet Ubiquitous Fluoride Congenitor: Binding Bifluoride in Triazolophanes Using Computer-Aided Design. *J. Am. Chem. Soc.* **2014**, *136*, 5078–5089.
56. Juwarker, H.; Lenhardt, J. M.; Pham, D. M.; Craig, S. L. 1,2,3-Triazole CH···Cl^- Contacts Guide Anion Binding and Concomitant Folding in 1,4-Diaryl Triazole Oligomers. *Angew. Chem., Int. Ed.* **2008**, *47*, 3740–3743.
57. Alunni, S.; Pero, A.; Reichenbach, G. Reactivity of Ions and Ion Pairs in the Nucleophilic Substitution Reaction on Methyl *p*-nitrobenzenesulfonate. *J. Chem. Soc., Perkin Trans. 2* **1998**, 1747–1750.
58. Frassineti, C.; Ghelli, S.; Gans, P.; Sabatini, A.; Moruzzi, M. S.; Vacca, A. Nuclear Magnetic Resonance as a Tool for Determining Protonation Constants of Natural Polyprotic Bases in Solution. *Anal. Biochem.* **1995**, *231*, 374–382.
59. McDonald, K. P.; Qiao, B.; Twum, E. B.; Lee, S.; Gamache, P. J.; Chen, C.-H.; Yi, Y.; Flood, A. H. Quantifying Chloride Binding and Salt Extraction with Poly(Methyl Methacrylate) Copolymers Bearing Aryl-Triazoles as Anion Receptor Side Chains. *Chem. Commun.* **2014**, 10.1039/C4CC03362K.
60. Alderighi, L.; Gans, P.; Ienco, A.; Peters, D.; Sabatini, A.; Vacca, A. Hyperquad Simulation and Speciation (Hyss): A Utility Program for the Investigation of Equilibria Involving Soluble and Partially Soluble Species. *Coord. Chem. Rev.* **1999**, *184*, 311–318.
61. Jackson, J. D. *Classical Electrodynamics*, 3rd ed.; Wiley: New York, 1998.
62. The ^{1}H NMR spectra collection with suppression of the solvent peak for the nondeuterated octanoic acid was only possible with the 50:50 mixture of CD_2Cl_2 into octanoic acid ($\varepsilon = 3$). In this solution, the binding affinities were found to be similar to pure CD_2Cl_2 (Figure S16). However, the stability of the ion pair, TBABr, was observed to increase (Figure S17). This ion pairing serves as a greater source of competition, and thus there is less of the actual complexed forms of the receptor in solution than when compared to pure dichloromethane.
63. Vander Griend, D. A.; Bediako, D. K.; DeVries, M. J.; DeJong, N. A.; Heeringa, L. P. Detailed Spectroscopic, Thermodynamic, and Kinetic Characterization of Nickel(II) Complexes with 2,2′-Bipyridine and 1,10-Phenanthroline Attained *via* Equilibrium-Restricted Factor Analysis. *Inorg. Chem.* **2007**, *47*, 656–662.
64. Juwarker, H.; Lenhardt, J. M.; Castillo, J. C.; Zhao, E.; Krishnamurthy, S.; Jamiolkowski, R. M.; Kim, K. H.; Craig, S. L. Anion Binding of Short, Flexible Aryl Triazole Oligomers. *J. Org. Chem.* **2009**, *74*, 8924–8934.
65. Li, Y.; Flood, A. H. Strong, Size-Selective, and Electronically Tunable C−H···Halide Binding with Steric Control over Aggregation from Synthetically Modular, Shape-Persistent [3_4]Triazolophanes. *J. Am. Chem. Soc.* **2008**, *130*, 12111–12122.
66. Li, Y. J.; Pink, M.; Karty, J. A.; Flood, A. H. Dipole-Promoted and Size-Dependent Cooperativity between Pyridyl-Containing Triazolophanes and Halides Leads to Persistent Sandwich Complexes with Iodide. *J. Am. Chem. Soc.* **2008**, *130*, 17293–17295.